Simultaneous EEG and functional MRI

van Houdt, P.J.

2013

document version
Publisher's PDF, also known as Version of record

CHAPTER 6

EEG-fMRI systematically compared to ECoG

Based on van Houdt PJ, de Munck JC, Leijten FSS, Huiskamp GJM, Colon AJ, Boon PAJM, and Ossenblok PPW (submitted). Understanding EEG-fMRI correlation patterns in presurgical evaluation of focal epilepsy

6.1 Introduction

Due to recent progress in the field of neuroimaging, epilepsy has become known as a network disease affecting different brain regions that are functionally interconnected (Richardson 2010; Lemieux et al. 2011; Laufs 2012). Especially for epilepsy surgery candidates the challenge is to characterize the different parts of the network and to determine their role during the generation and propagation of epileptiform activity (Vulliemoz et al. 2009). It has been suggested that EEG-fMRI is a suitable noninvasive technique to reveal these epileptiform networks (Kobayashi et al. 2006b; Rosenkranz et al. 2010; Chaudhary et al. 2011); EEG-fMRI reveals regions of BOLD changes that are associated with (inter)ictal epileptiform activity observed in the simultaneously recorded EEG. This technique enables the detection and visualization of multiple activated areas and does not depend on source reconstruction models, such as required with scalp EEG or MEG. Until now, EEG-fMRI in epilepsy has mainly been used as a research tool to increase our understanding of epileptic phenomena. Recently, a potential role of EEG-fMRI in the preoperative evaluation has been suggested, for example, by using EEG-fMRI to guide invasive electrode placement (Zijlmans et al. 2007) or to predict surgical outcome (Thornton et al. 2010a). The latter suggestion

was based on the results of ten patients indicating that EEG-fMRI correlation patterns with significant BOLD regions remote from the seizure onset zone were associated with a less favorable surgical outcome.

The added value of EEG-fMRI in clinical practice still needs to be established by evaluation relative to a gold standard. The majority of the papers about EEG-fMRI in focal epilepsy used noninvasive gold standards for the evaluation: (1) the presumed seizure focus based on clinical information and other noninvasive investigations (e.g. Salek-Haddadi et al. 2006; Hawco et al. 2007; Lemieux et al. 2007; Liu et al. 2008), (2) the scalp topography of IEDs in the co-registered EEG (e.g. Kobayashi et al. 2006b; Zijlmans et al. 2007; Jacobs et al. 2009; Moeller et al. 2009; van Houdt et al. 2010a), (3) EEG source localization outside the scanner (e.g. Bagshaw et al. 2006; Grova et al. 2008), or (4) the relation to the location of the lesions of the patients (Tyvaert et al. 2008a). Until recently, the number of studies that compared EEG-fMRI to invasive EEG recordings or postoperative results was limited; most of them describe the results for a few cases (Lazeyras et al. 2000; Bénar et al. 2006; Zijlmans et al. 2007; Moeller et al. 2009; Vulliemoz et al. 2009; Vulliemoz et al. 2010; Pittau et al. 2011; van Houdt et al. 2012). Four studies with larger patient populations ($n > 10$) have been published that compared EEG-fMRI to the seizure onset zone determined from invasive EEG recordings (Grouiller et al. 2011; Thornton et al. 2011; Pittau et al. 2012; Hauf et al. 2012). All these studies demonstrated that one of the significant BOLD regions was concordant with the seizure onset zone in the majority of the patients. The study of Grouiller et al. (2011) showed a better concordance for lateral temporal or extratemporal neocortical epilepsy compared to mesial temporal lobe epilepsy. Furthermore, Pittau et al. (2012) showed that in 64 % of the patients in whom a BOLD response was obtained, EEG-fMRI provided additional information with respect to scalp EEG alone.

Although the EEG-fMRI correlation pattern includes the seizure onset zone in most cases, it has often been reported that the correlation pattern consists of multiple activated brain regions (e.g. Salek-Haddadi et al. 2006; Vulliemoz et al. 2009; Pittau et al. 2012). Therefore, the question arises: How to interpret these multiple brain regions? Since most EEG-fMRI studies reveal the presumed networks related to interictal epileptic activity, a first logical step in the validation process of EEG-fMRI is the comparison with interictal events recorded with invasive EEG. To our knowledge this has not been investigated for a larger patient population yet. Possible explanations are that patients are only implanted with intracranial EEG when the noninvasive results are inconclusive and that the spatial sampling of invasive EEG is limited. The goal of this study is to systematically evaluate the EEG-fMRI findings for presurgical candidates who all underwent preoperative ECoG recordings. The results are viewed from two perspectives. The first perspective is the EEG-fMRI perspective, where the goal is to determine whether the regions of significant BOLD are related to onset and/or propagation of interictal epileptic activity in invasive EEG

recordings. Second, from a clinical point of view in which we investigate to what extent information is missed with EEG-fMRI analysis compared to the distribution of IEDs in the ECoG data. Furthermore, EEG-fMRI correlation patterns are related to the clinically more relevant seizure onset zone, cf. Thornton et al. (2011).

6.2 Methods

6.2.1 Patients

In this study, 16 patients (8 male, age 25.1 ± 8.2, Table 6.1) with refractory epilepsy were included who were candidates for epilepsy surgery guided by either acute or chronic subdural ECoG recordings. The inclusion criteria were (1) EEG-fMRI analysis yielded at least one area of significant BOLD; (2) interictal ECoG data were available; (3) CT scans or digital intra-operative images were available to determine the positions of the implanted electrodes. Table 6.1 summarizes the subjects' demographic and clinical details. All patients showed MRI visible lesions, except patient 5 and 12. Electrode placement was based on the electroclinical hypothesis (column 4, Table 6.1) determined from the results of noninvasive preoperative work-up. Patient 5 was not operated due to the presence of a multifocal seizure onset zone overlapping with functional areas, whereas patient 10 was not operated due to complications on the second day of subdural grid recordings. The EEG-fMRI study was approved by the Medical Ethics Committee of the University Medical Center Utrecht and VU University Medical Center and all patients gave informed consent.

6.2.2 Acquisition of EEG-fMRI data

EEG-fMRI data were acquired at three institutes (Kempenhaeghe [KH], Heeze; University Medical Center Utrecht [UMCU], Utrecht; VU University Medical Center [VUmc], Amsterdam). The patients were asked to lie relaxed with their eyes closed during the recording. The length of the fMRI recordings varied between 20 to 45 min depending on the subject's endurance. At KH and UMCU the same protocol was used: 3 T MR scanner (Achieva, Philips Medical Systems, Best, The Netherlands); T_2^*-weighted EPI sequence; TR = 2.5 s; TE = 35 ms; reconstructed voxel size $3.2 \times 3.2 \times 3\,\mathrm{mm}^3$; 31-33 adjacent slices; bottom-to-top slice order (patients 1, 2, 4, 8, 9, 10, and 14) or interleaved slice order (patients 3, 5, 6, 11, 12, 15, 16). Patients 7 and 13 were scanned at a 1.5 T MR scanner (Magnetom Sonata, Siemens, Erlangen, Germany) in VUmc with the following parameters: TR = 3 s; TE = 60 ms; reconstructed voxel size $3.3 \times 3.3 \times 3\,\mathrm{mm}^3$; 24 slices with a 10% gap; bottom-to-top slice order.

For each patient an anatomical T_1-weighted scan was available for the visualization of the EEG-fMRI results. All institutes used the same MR-compatible EEG amplifier (MicroMed, Treviso, Italy) to acquire EEG data during scanning. EEG was recorded using a 32-channels (UMCU) or 64-channels EEG cap (KH, VUmc) positioned according

Table 6.1: Summary of demographic and clinical details.

Patient	Age /Sex	MRI abnormalities	Lateral-ization	Electroclinical Hypothesis	Seizure onset zone	Resected Area	Engel Score	Pathology
1	25F	PO tumor	L	TO onset with propagation to T	mT, lT	TO	1A	astrocytoma
2	24M	T cavernoma	L	T	-	T	1D	cavernoma
3	13F	TSC	L	F	bilateral F	F	4B	Tuber
4	41M	mF dysplasia	R	F	mF	mF	1A	Dysplasia
5	34M	Negative	L	O onset with propagation to T, C, and mF	O, P, T	no operation	no operation	no operation
6	23M	Deep white matter abnormality in right hemisphere	R	F or TO	mF, F, P, C	F	3A	MCD
7	30F	mF lesion	R	mF	mF, F	mF	4B	MCD
8	22F	mT dysplasia	L	T posterior or anterior	T basal	T	1A/B	MCD
9	33F	P dysplasia in operculum	L	PC	FC	PC	2B	FCD
10	17M	Resection based on PO gangliocytoom	L	PO	no conclusion	no operation	no operation	no operation
11	28M	Enlargement of right ventricle	R	T posterior	T, mT	T	1B	normal
12	19F	Negative	L	mF or lF	F	F	1A	normal
13	23M	prefrontal resection based on DNET	R	F	mF, P, C	F	3A	DNET
14	12F	MTS; T differentiation gray/white matter	L	T	-	T	1A	MTS
15	31F	Suspicion of mild cortical dysplasia	R	TO	mT, T	T	1A	MCD
16	16M	T tumor	L	T	-	T	3A	ganglioglioma

Abbreviations: Sex: M = male; F = female. MRI abnormalities: m = mesial; F = frontal; P = parietal; O = occipital; T = temporal; MTS = mesial temporal sclerosis; TSC = tuberous sclerosis complex; DNET = Dysembryoplastic neuroepithelial tumor; Lateralization: L = left; R = right; Electroclinical hypothesis: m = mesial; l = lateral F = frontal; P = parietal; C = Central; O = occipital; T = temporal; Seizure onset zone: based on ECoG recordings; only determined for patients with chronic ECoG recordings; Engel Score: follow-up > 1 year after surgery. Pathology: DNET = Dysembryoplastic neuroepithelial tumor; MCD = malformations of cortical development; FCD = focal cortical dysplasia, Taylor-type; MTS = mesiotemporal sclerosis

to an extended 10-20 system with a sampling rate of 1024 Hz (UMCU) or 2048 Hz (KH, VUmc). ECG was co-registered either as a bipolar signal included in the EEG data (KH, UMCU) or as a separate data file with MR compatible sensors (VUmc).

6.2.3 Acquisition of ECoG data

ECoG data were either acquired during surgery (acute ECoG, n = 4) or prior to surgery (chronic ECoG, n = 12) at UMCU. The recording was performed with subdural grids or strips (Ad-Tech, Racine, QI, USA and Brain-electronics, Houten, the Netherlands) consisting of platinum or stainless steel electrodes with an interelectrode distance of 1 cm (for more details see Agirre-Arrizubieta et al. (2009)).

Those patients who received chronic ECoG were implanted with 80 - 120 electrodes (patients 1, 3, 5-13, 15). The data were acquired with a sampling rate of 512 Hz and filtered between 1 and 70 Hz. For each patient, a 10 min ECoG sample was selected during awake rest, at least one hour after a seizure. This epoch was selected in such a way that all visually identified IED-types were present and that there was a balance between normal background ECoG and IEDs (i.e. no abundance of IEDs). The positions of the electrodes were determined by matching a post-implantation CT image to the anatomical MRI acquired during EEG-fMRI recording using Brain Imaging Analysis Package[1]. An MRI surface rendering was created of the brain and the electrode positions and labels were manually determined using the point toolbox of the software, such that each electrode was known in MRI coordinates.

Four patients underwent acute ECoG during surgery (patient 2, 4, 14, 16). A grid with 20 electrode contacts was used in all patients, while in patients 14 and 16 also a subdural strip of 8 contacts was placed. The grid was replaced several times during the recording. For each patient, at least one epoch of data was available that lasted more than 5 min (sample rate 2048 Hz) during which the position of the grid did not change. The positions of the grid and strip were based on digital pictures taken before and after electrode placement. The overlap between sulci and gyri on the pictures and the surface rendering of the anatomical scan was determined visually, such that the positions and labels of the electrodes could be indicated at the anatomical scan.

6.2.4 EEG-fMRI analysis

The analysis of the EEG-fMRI data was performed with the Brain Imaging Analysis Package, similar to the procedures described in van Houdt et al. (2012). Briefly, EEG data were corrected for image artifacts and pulse artifacts using the methods as described by de Munck et al. (2013). From the EEG, a reference function was extracted representing the timing of IEDs during the EEG-fMRI acquisition. Separate reference

[1] http://demunck.info/software/

functions were created for IEDs with different shape or topology assuming that these different IED-types have different sources. The reference function was correlated to the preprocessed fMRI data through a GLM framework. Studies in epilepsy patients have shown that the shape of the HRF varies among patients (Jacobs et al. 2009). In fact, the peak time of the HRF may have localizing value towards the onset site of the IEDs (Hawco et al. 2007; Jacobs et al. 2009; Pittau et al. 2011). Therefore, the parameters of the HRF were estimated from the data using a FIR model (de Munck et al. 2007) instead of using a set of fixed HRFs. An F-test was used to calculate the level of correlation between the data and the reference function, while taking the number of estimated parameters, the number of confounders and the number of data points into account. The resulting p-values were converted to FDR-values (Genovese et al. 2002), which was used to threshold the statistical maps (FDR < 5 %). Thereafter, a cluster algorithm was applied to visualize differences in the shape of the HRF for different brain regions. The voxels within a single cluster were indicated with the same color as the corresponding average HRF. Clustering was truncated based on visual inspection when further subdividing did not yield more variation. We used this clustering approach to explore whether the shape of the HRF yields more information about the functional role of an area (i.e. related to onset or propagation of epileptic activity).

6.2.5 ECoG analysis

To investigate whether the significant BOLD regions overlap with the regions that are active during the IEDs occurring in ECoG data, a semi-automatic procedure was applied for the analysis of these ECoG data. This procedure facilitates an objective comparison with EEG-fMRI correlation patterns and results in (1) a spatial pattern indicating which electrodes were involved during the occurrence of IEDs in the ECoG data, and (2) an onset pattern indicating at which electrodes the activity was first visible. Mathematical details about the method are described in the appendix.

The estimation of the spatial pattern is based on the semi-automatic analysis developed for stereo-EEG data as presented in van Houdt et al. (2012). For that purpose, a nonlinear association analysis (Lopes da Silva et al. 1989; Pijn et al. 1990; Wendling et al. 2001) was performed for nonoverlapping sliding window of 2.5 s (Figure 6.1, step 1), yielding for each window k and for each pair of electrodes (i, j) a maximal association value $h^2_{ij}(k)$ and a corresponding time delay $\tau_{ij}(k)$ (Figure 6.1, step 2). Thereafter, an average association value was computed for each electrode, called the association strength, representing the association of that electrode relative to the other electrodes (Figure 6.1, step 3). Next, a regression analysis was performed to investigate which changes in association strength time series can be explained by the occurrence of IEDs (Figure 6.1, step 5). This model used the association strength as explained variable (similar to the fMRI signals in EEG-fMRI analysis) and

the IEDs in the data as predictor (Figure 6.1, step 4). The advantage of this method is that it does not require a selection of specific background windows. The resulting correlation value indicates to what extent a certain electrode is involved during IEDs relative to the other electrodes (Figure 6.1, step 6). This involvement is indicated with color-coded dots scaled by the correlation value; nonsignificant correlations are indicated in black (FDR > 5 %). A spatial pattern is called significant if FDR < 5 % for at least one electrode. If multiple IED-types were present in the data, the analysis was performed for each IED-type separately, yielding multiple spatial patterns.

The spatial pattern only indicates which ECoG electrodes were more active during IEDs, but it is also important to determine the electrodes at which the epileptiform activity first becomes apparent, the onset of the IEDs. Therefore, the second part of the analysis consists of the estimation of an onset pattern (Figure 6.1, step 7-9). Time delays $\tau_{ij}(m)$ between two electrodes i and j can be interpreted as the direction of information flow between two signals (Wendling et al. 2001). For that purpose, the nonlinear association analysis was performed for windows of 1 s centered around the IEDs (Figure 6.1, step 7), and the delays $\tau_{ij}(m)$ were subsequently used to estimate the moment in time at which an IED was measured at each electrode (Figure 6.1, step 8). For each single IED a temporal pattern was estimated. An example is shown in step 9 of Figure 6.1 together with the corresponding IED. The color-coding indicates the electrodes associated with the early onset of a particular IED (bright colors) with respect to other electrodes (red/black).

6.2.6 Comparison of EEG-fMRI and ECoG results

Since EEG-fMRI and ECoG have different spatial domains (voxels vs. electrodes), concordance was determined at the level of the underlying anatomical brain regions. The clinical rationale for this approach is that in neurosurgical practice areas are resected that are defined by gyri and sulci. Therefore, a digital atlas of the brain was matched to the anatomical MRI such that the activated areas could be automatically linked to the corresponding anatomical regions. We used the anatomic automatic labeling (AAL) atlas (Tzourio-Mazoyer et al. 2002) available from the MRIcron software[2]. The AAL brain areas (n = 90) were grouped in ten larger brain regions for each hemisphere (Agirre-Arrizubieta et al. 2009): lateral temporal region (TL); mesial temporal region (TM); inferior, medial, and superior frontal gyri (FL); orbitofrontal region (FO); interhemisperic region (IH); central region (C); parietal region (P); occipital region (O); basal ganglia and thalamus (B); insular region (Ins). As a result, the corresponding anatomical brain regions were determined for each HRF cluster of EEG-fMRI and for each significantly activated ECoG electrode. HRF clusters that were not located in one of these brain regions (e.g. in white matter, cerebellum, or ventricles) were discarded from further analysis, indicated by symbol ∅.

[2] www.mccauslandcenter.sc.edu/mricro/mricon/

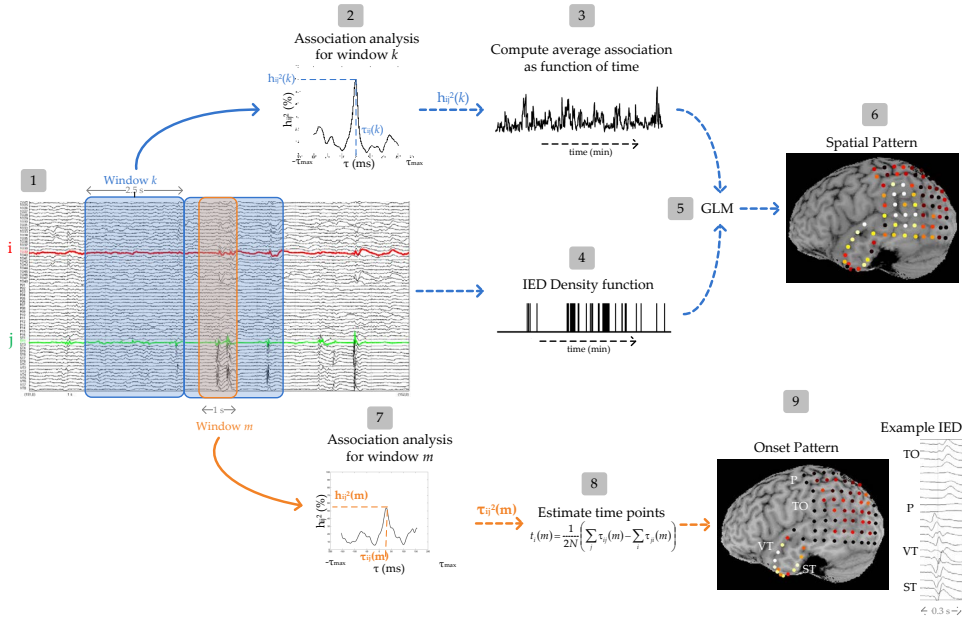

Figure 6.1: Flow chart of ECoG analysis consisting of two steps: estimation of spatial correlation pattern (step 1 to 6) and the estimation of an onset pattern (step 7-10).

First, the level of concordance was determined from an EEG-fMRI perspective; the overlap was determined between each HRF cluster and the spatial and temporal ECoG patterns following the terminology of Salek-Haddadi et al. (2006) and Lemieux et al. (2008) (Figure 6.2). The term *concordance* (C) was used when the HRF cluster was located in the same brain regions as active ECoG electrodes in the spatial pattern. Subsequently, for each concordant HRF cluster, it was determined whether this cluster was also concordant with the early onset of the IEDs as visualized with the temporal ECoG pattern. The term *concordance plus* (C+) was used to indicate that there was not only overlap between the HRF cluster of EEG-fMRI and the active ECoG electrodes, but also remote activations were obtained with EEG-fMRI analysis. Finally, D indicates discordant areas when EEG-fMRI areas had no ECoG match and U (= *unknown*) was used for EEG-fMRI areas that had not been sampled with subdural grids or strips.

Second, the level of concordance was assessed from an ECoG perspective; it was determined whether the brain regions with significantly activated ECoG electrodes had an EEG-fMRI counterpart. If so, this area was called a true positive EEG-fMRI cluster. If not, the area was counted as a false negative area. These numbers were used to

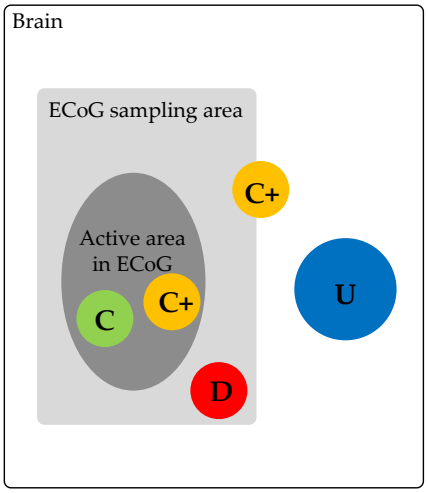

Figure 6.2: Schematic representation of the determination of concordance between EEG-fMRI and ECoG results. Each color represents a different HRF cluster, hence areas with the same color belong to the same cluster having a similar shape of the HRF. C = concordance (green cluster), C+ = concordance plus (orange cluster), D = discordance (red cluster), U = unknown (blue cluster).

determine for each data set whether all active ECoG brain regions were revealed by EEG-fMRI analysis (i.e. no false negatives), only part of the active brain regions (i.e. at least one true positive), or none (i.e. no true positives, only false negatives). This was performed separately for the spatial and onset ECoG patterns.

6.3 Results

6.3.1 General Results

The IEDs identified in the EEG during fMRI consisted of one IED-type for almost all patients, except for patient 14 in whom two IED-types were identified in the EEG, resulting in 17 IED-correlated fMRI analyses. Each analysis revealed multiple activated BOLD areas. For each patient, clustering of the estimated HRFs of these significant BOLD regions resulted in three to six clusters with varying shape and sign of the average HRF. EEG-fMRI findings were compared to the spatial and onset patterns of IEDs occurring in the ECoG data. In most ECoG data sets, multiple IED-types were present, but the regression analysis yielded only significant spatial and onset patterns for frequently occurring or widespread IEDs. Significance was not reached for IEDs that occurred sporadic or that were present at only one or two electrode

contacts. For patient 16, ECoG analysis did not reveal any significant results, because too little contrast was present to reach significance in the regression analysis due to continuous spiking in the ECoG data.

6.3.2 EEG-fMRI perspective

An illustrative case showing the concordance between EEG-fMRI and ECoG is patient 1, presented in Figure 6.3. In this patient, EEG-fMRI analysis of the IEDs identified during scanning (Figure 6.3a) yielded significant BOLD areas in the left lateral temporal region, in the left parietal region near the lesion of the patient (Figure 6.3b), and in the left thalamus (insert Figure 6.3c). Clustering of the HRFs in these significant voxels showed that each EEG-fMRI area is characterized by a different HRF (Figure 6.3c and d). Positive HRF clusters were obtained in the left thalamus and left lateral temporal region (cluster 1, 2, 3 in Figure 6.3d), while negative HRFs were found in the left posterior temporal region and parietal region (cluster 5 and 6 in Figure 6.3d). Cluster 4 was not located in one of the specified brain regions (edge of the brain). Electrode grids were implanted across the temporal and parietal lobes (Figure 6.3f), covering the HRF clusters 2, 5, and 6. Figure 6.3e shows the IEDs that were marked in the ECoG data, which were comparable to the IEDs of the EEG-fMRI recording. The spatial pattern (Figure 6.3f) shows maximal activity in the left frontotemporal and left parietal region, showing overlap with the EEG-fMRI areas. Furthermore, the estimated onset of the IEDs was located at the lateral temporal electrodes (Figure 6.3g). Therefore, of the spatially concordant HRF clusters (cluster 2, 5, and 6), only the positive HRF cluster (cluster 2 in Figure 6.3d) was also concordant with the early onset areas of the IEDs in ECoG.

Results of the other 15 patients are presented in Figure 6.4 showing for each patient the HRF clusters (first column) and the spatial and onset ECoG patterns (second and third column). EEG-fMRI and ECoG results were displayed in such a way that all implanted electrodes and almost all significant EEG-fMRI areas are visible, but at least those EEG-fMRI areas that were concordant with ECoG and the resection area (indicated by the white contour line). For most patients, a surface rendering was the optimal choice to visualize the EEG-fMRI and ECoG data. In patient 4 and 8 a slice view was chosen, because the deep interhemispheric activity (patient 4) and bilateral temporal activity (patient 8) impeded a fair visualization of the results at a surface render. To systematically present the HRF clusters, warm colors (red, yellow, orange) were used to indicate positive HRF clusters; cold colors (blue, green) were used to indicate negative HRF clusters. In most patients, more than one IED-type was visually identified in the ECoG data, but only those spatial and onset patterns are shown that are concordant with the EEG-fMRI correlation pattern (second and third column of Figure 6.4). Spatial and onset patterns in one row correspond to the same IED-type. In patients 8, 11, and 15, the EEG-fMRI results were partially concordant with two IED-types in the ECoG data. Since the spatial patterns of these IED-types were

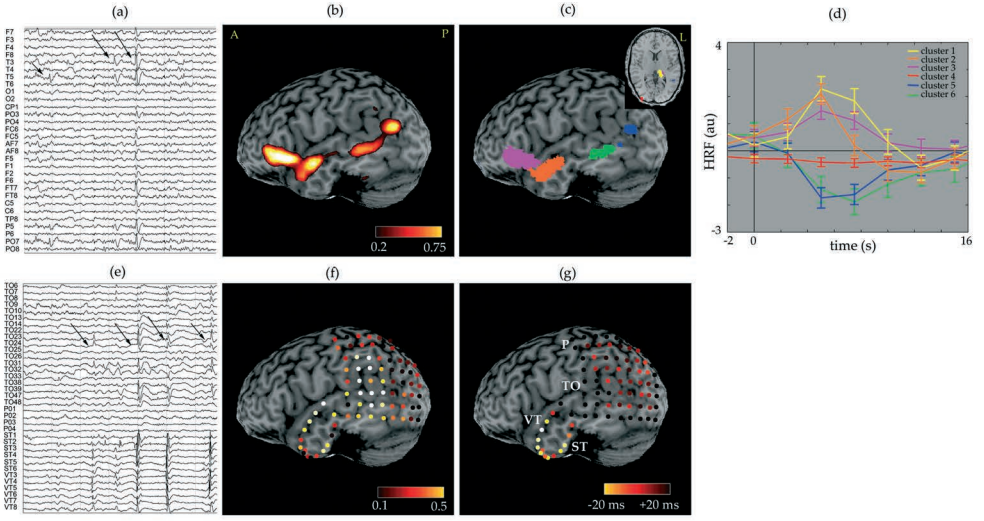

Figure 6.3: Illustrative case showing the EEG-fMRI results (top row) and ECoG results (bottom row) for patient 1. (a) shows the IEDs identified during EEG-fMRI. (b) shows the correlation pattern resulting from the fMRI analysis. In (c) the results of the HRF clustering are shown; each color corresponds to a different cluster and a different average HRF shown in (d). (e) shows the IEDs identified in the selected ECoG data. (f) represents the spatial correlation pattern from the ECoG analysis, while (g) represents the onset pattern of the IEDs in the ECoG data.

classified as different (i.e. involve different electrodes), both patterns were shown. Furthermore, each onset pattern corresponds to a single IED, but was representative for all IEDs of the same IED-type. Only in patient 6, three separate onset patterns were visually identified. For patient 3, the onset patterns were highly variable, therefore, no onset patterns were shown for this patient. We refer to Table A.1 for a complete summary of all data.

Figure 6.4 illustrates that for 15 of the 17 data sets the EEG-fMRI clusters overlapped with the spatial pattern of at least one IED-type in the ECoG data. Note that, concordance was defined in terms of anatomical brain regions and that in some data sets (e.g. patient 8 and 12) visual inspection of the data shows that the overlap is not exact. In 4 data sets (patients 2 - 5), one of the HRF clusters was spatially concordant with the IEDs in ECoG. In 11 datasets (patients 1 (see Figure 6.3), 6 - 14.1, 15), two or three HRF clusters were concordant with the spatial ECoG pattern. At least one of them was also concordant with the onset of the IEDs. In some patients (patients 1, 4, 7, 10 and 16) HRF clustering clearly distinguishes the onset region from propagation areas as a single cluster of neighboring voxels. In the other patients, clusters were more widespread and usually involved other brain regions as well (Patients 5, 6,

Table 6.2: Summary of the concordance from an EEG-fMRI perspective. For each HRF cluster it was determined whether it was concordant (C/C+) with the spatial or onset pattern of IEDs in ECoG data, discordant (D), or whether it was not covered by subdural grids (U). Furthermore, the overlap with the resection area was determined. A distinction was made between clusters with a positive HRF and clusters with a negative HRF.

EEG-fMRI	ECoG			Resection Area
	C/C+ spatial (onset)	D	U	
Positive HRF cluster	19 (14)	1	9	13
Negative HRF cluster	14 (8)	0	12	8

11, 13, and 15). In those patients, the spatial patterns of the ECoG data were widely distributed as well. Only one HRF cluster was classified as discordant (patient 5). Furthermore, in all data sets HRF clusters were obtained that were not covered with electrodes, so that their function in the network could not be verified. In data set 14.2 none of the HRF clusters was covered by invasive electrodes.

Results of patient 1 (Figure 6.3) suggest different roles for the different parts of the network, because all three HRF clusters are spatially concordant with the electrical ECoG activity, while only one of them is related to the early onset of the IEDs. To examine whether the shape of the HRF is predictive for the level of concordance, we investigated the sign of the HRF for each cluster in relation to the level of concordance. Results are summarized in Table 6.2, showing that 19 positive HRF clusters were spatially concordant with a spatial ECoG pattern. Of those 19 clusters, 14 were also concordant with the early onset of IEDs. On the other hand, also 14 negative HRF clusters were concordant and 8 of them were concordant with the early onset. Note that many "unknown" HRF clusters were observed, either with a positive or a negative HRF. Finally, 13 positive HRF clusters and 8 negative HRF clusters were located in the resection area.

6.3.3 Clinical Perspective

From a clinical perspective it is important to know whether EEG-fMRI overlaps with the interictal findings of ECoG data and, ultimately, whether it overlaps with the seizure onset zone. Table 6.3 shows a comparison between all findings (EEG-fMRI clusters, interictal spatial and temporal ECoG patterns, seizure onset zone, and resected area) by counting the number of data sets in which each combination of findings was concordant. Table 6.3 illustrates that EEG-fMRI clusters overlap partially with the spatial ECoG patterns in all data sets. In 8 of these data sets (50%), the EEG-fMRI clusters included all significantly activated ECoG electrodes for all different IED-types. In the other 8 data sets, EEG-fMRI clusters overlapped with the spatial pattern of only one of the IED-types present in the ECoG data (e.g. patient 9) or

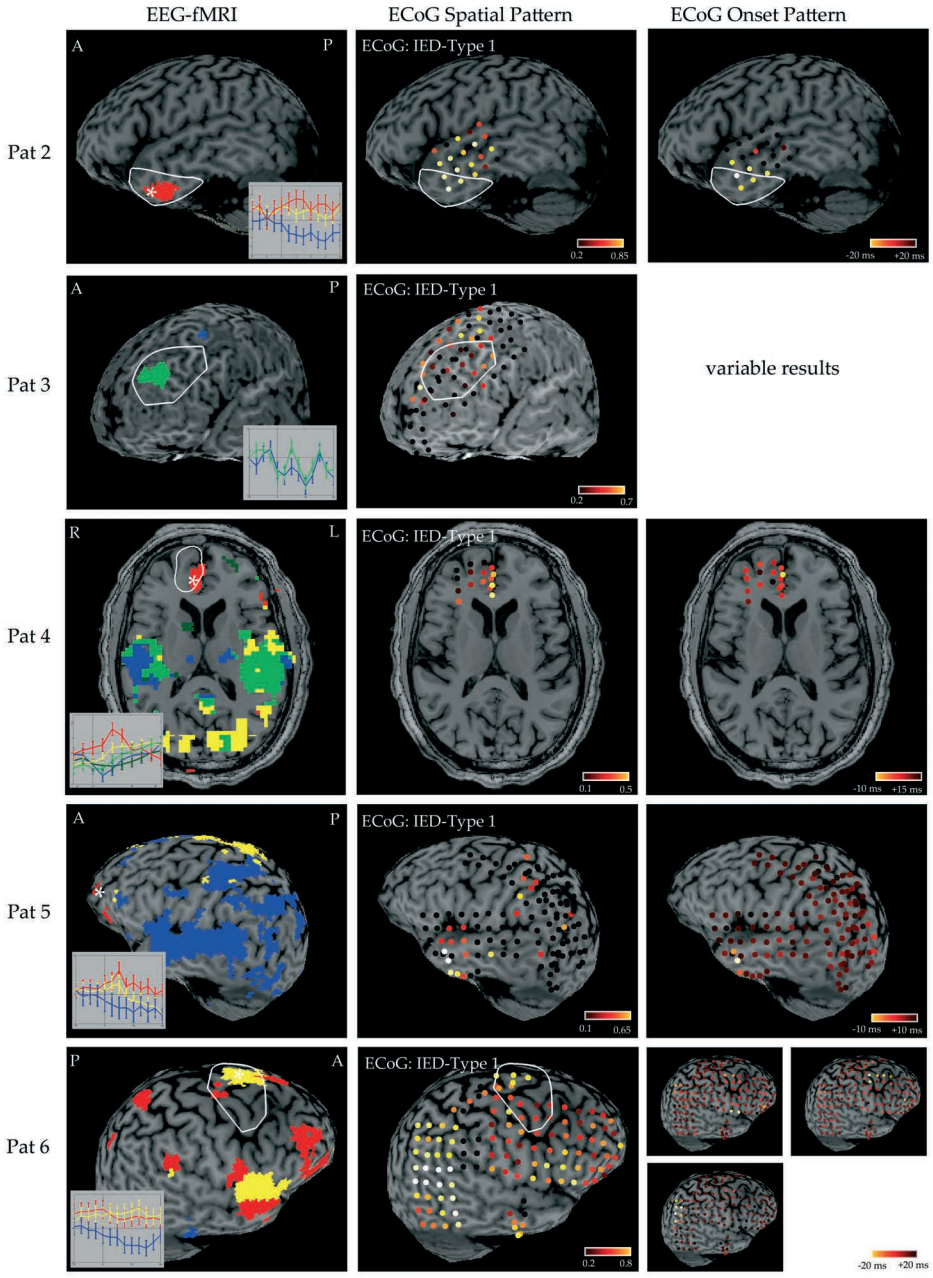

Figure 6.4: EEG-fMRI (first column) and ECoG results (second and third column) of all patients. The colors of the EEG-fMRI clusters correspond to the HRF time courses, where positive clusters are indicated with warm colors (red, yellow, orange) and negative clusters with cold colors (blue, green). The white contour line indicates the resection area. The white asterisk indicates the location of the maximal *F*-statistic of the positive responses, in case this was visible in the chosen view. Abbreviations: n.a = not available.

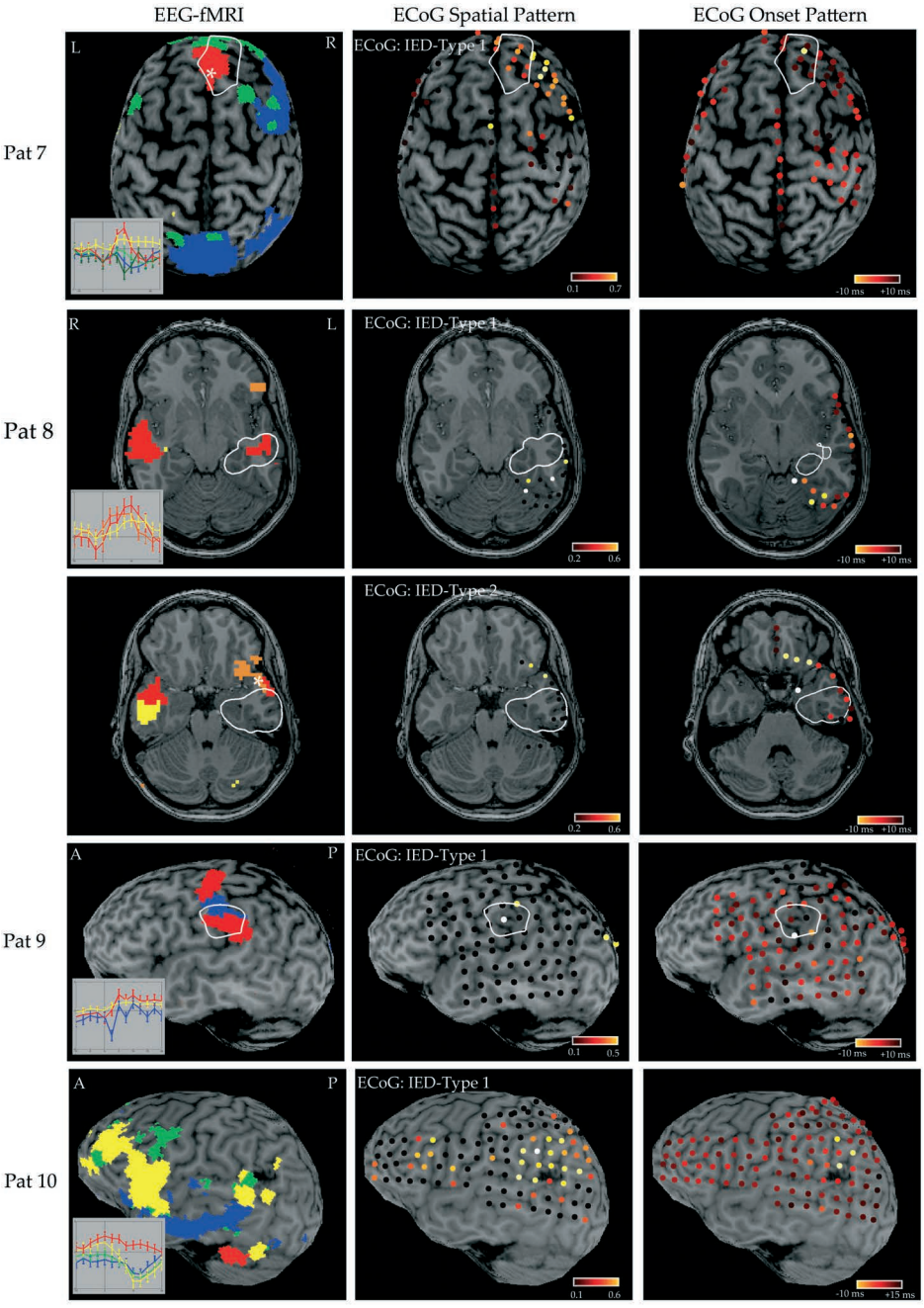

Figure 6.4: Continued

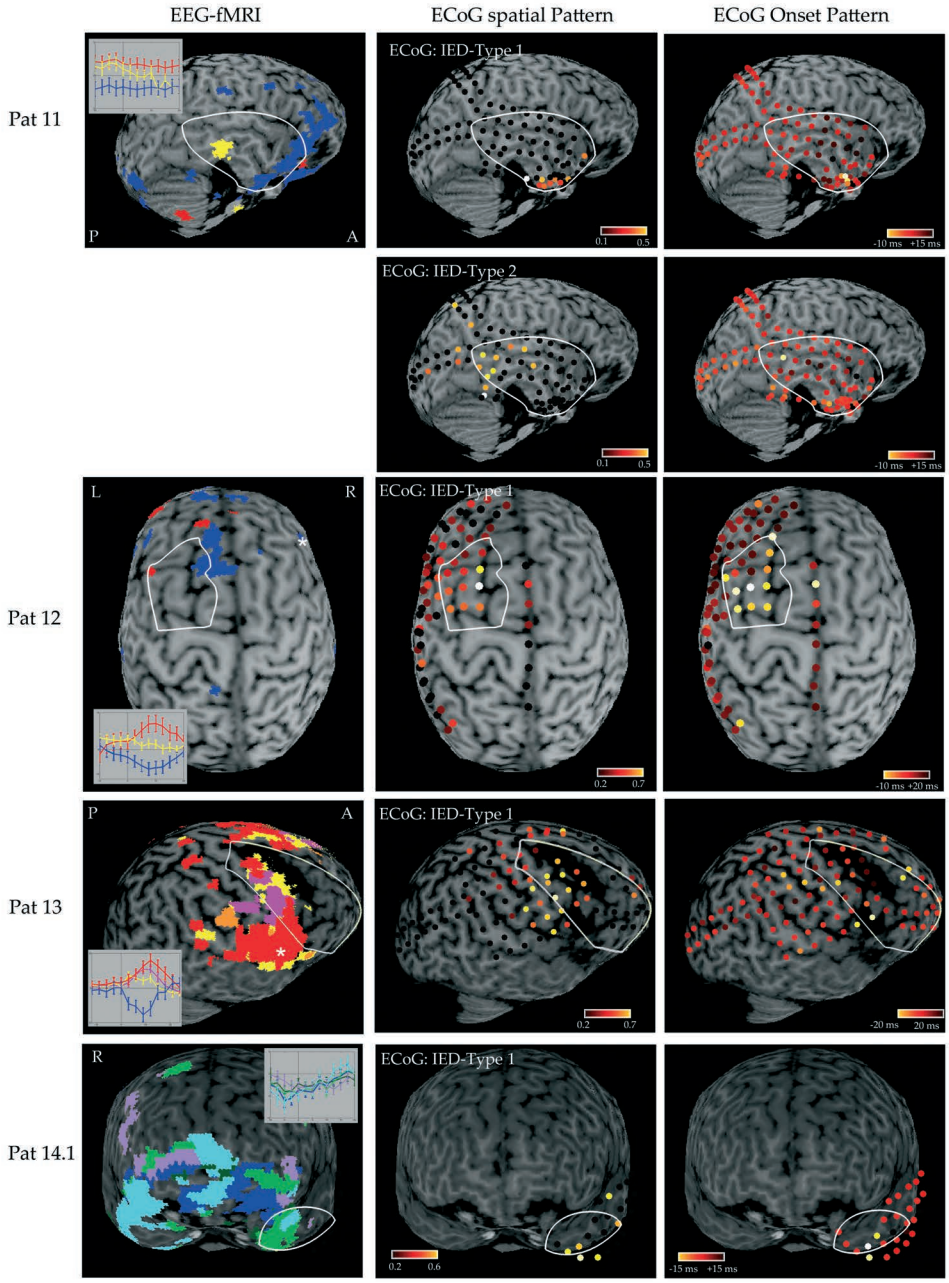

Figure 6.4: Continued

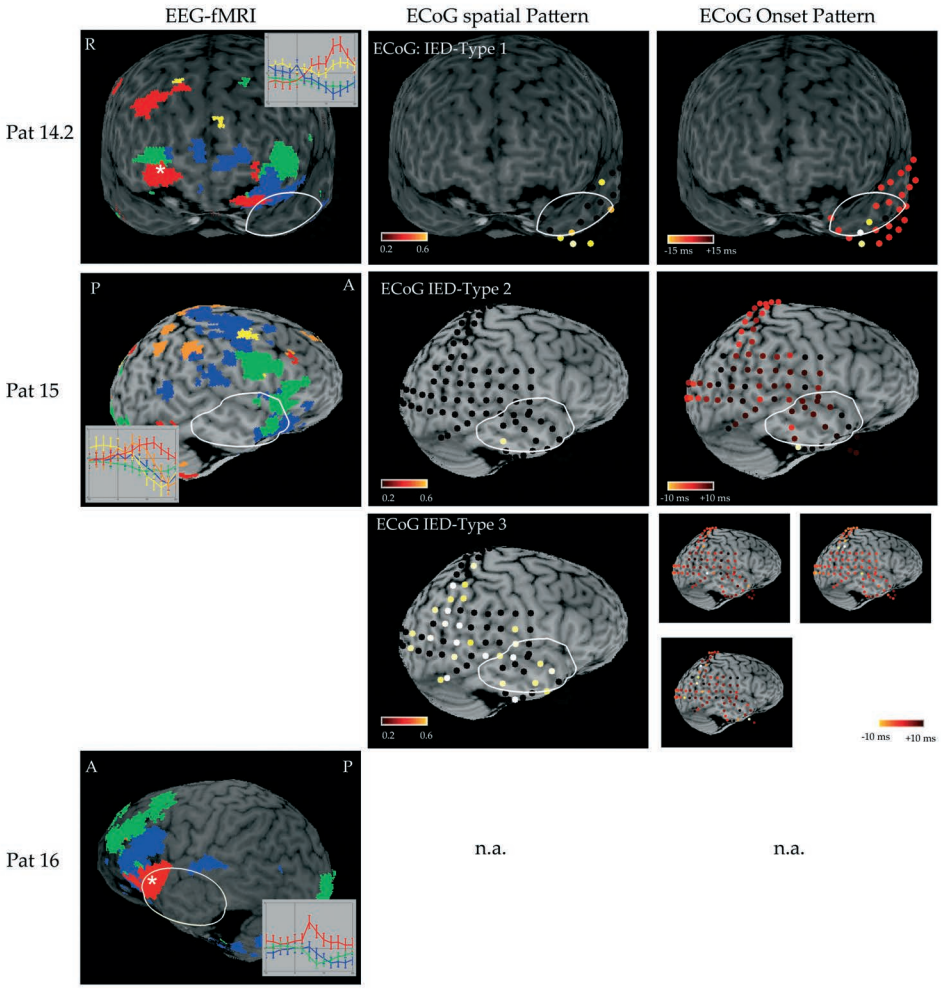

Figure 6.4: Continued

an EEG-fMRI cluster was found close to the active ECoG electrodes, but was located in another brain region, such as in patient 10, in whom an EEG-fMRI cluster was found just below the lesion in the posterior part of the temporal lobe, whereas ECoG activations were found above the lesion in the parietal lobe. EEG-fMRI clusters were concordant with the early onset of one of the ECoG IED-types in 88 % of the data sets, whereas they were concordant with the distinct onset areas of all IED-types in 69 % of the data sets. Furthermore, EEG-fMRI clusters included the complete seizure onset zone in 83% of the data sets in which the seizure onset zone was determined. In patient 3, only the left frontal region showed up in EEG-fMRI, while the seizure onset zone was determined bilaterally in the frontal lobe. For patient 6, only EEG-fMRI activations were found in the frontal region and not in the parietal and central regions. In 93 % of the data sets, at least one EEG-fMRI cluster was located within the resection area. Moreover, this particular EEG-fMRI cluster was the same cluster that was also concordant with the onset of the IEDs in 12 data sets.

The interictal spatiotemporal ECoG patterns (second and third row in Table 6.3) were also compared to the seizure onset zone and resection area. A general finding in all data sets was that the temporal pattern is a subset of the spatial pattern. In other words, the electrodes that reflected the early onset of the IEDs, were also the electrodes that were involved in the spatial ECoG pattern. In 75 % of the data sets the interictal spatiotemporal patterns included the complete seizure onset zone. In patients 3, 5, and 13, the interictal results only reflected part of the seizure onset zone. In 6 data sets the interictal spatial pattern was larger than the seizure onset zone. In all patients that were operated on and in whom ECoG data were analyzed ($n = 14$), part of the interictal spatiotemporal patterns was located within the resected area. Finally, in 9 data sets (81 %) the complete seizure onset zone was removed, while only part of the seizure onset zone was removed in patients 6 and 13 and a lesionectomy was performed in patient 1, which did not include the seizure onset zone. The Engel score (> one year after surgery) was 1 or 2 for 9 patients, while the Engel score was 3 or 4 for 5 patients. No clear distinction was found between the EEG-fMRI results of patients with a good or poor surgical outcome: in both patient groups, EEG-fMRI correlation patterns were found that were widespread or focal and with either a positive or negative HRF.

6.4 Discussion

To our knowledge, this study is the first that systematically assessed the concordance between EEG-fMRI and the interictal spatiotemporal patterns as determined with ECoG for a large patient population. Our results confirmed that in most patients the EEG-fMRI pattern consisted of multiple activated regions (e.g. Vulliemoz et al. 2009; Pittau et al. 2012). Of the 16 patients studied a single focal region was found only in 4 of them (Patients 2, 3, 9, and 12). In all patients at least one EEG-fMRI cluster

Table 6.3: Concordance from a clinical perspective. A comparison is made between the EEG-fMRI clusters, interictal spatial and onset patterns of ECoG data, the seizure onset zone, and resected area by listing the percentage of concordant data sets. For the EEG-fMRI clusters compared to the spatiotemporal ECoG patterns, concordance is either counted when at least one of the active ECoG regions was obtained with EEG-fMRI (first number) or all ECoG regions (second number). For one patient the spatial and onset patterns were not computed (patient 16), whereas the seizure onset zone was only determined for the patients who received chronic ECoG (n =12) and 2 patients were not operated.

		ECoG		Seizure Onset Zone	Resection Area
		Spatial (n = 16)	Onset (n = 16)	(n = 12)	(n = 15)
EEG-fMRI clusters	(n = 17)	100% (50%)	88% (69%)	83%	93%
ECoG Spatial	(n = 16)	-	100%	75%	100%
Onset	(n = 16)	-	-	75%	100%
Seizure onset zone	(n = 12)	-	-	-	81%

was concordant with electrodes that were active during the occurrence of IEDs in the ECoG data, some of which are related to the onset and others to propagation of IEDs. In addition, the extent of the EEG-fMRI correlation pattern seems an indicator for the extent of the interictal spatial pattern; when the EEG-fMRI correlation pattern was widespread without clear HRF clustering, the ECoG spatial patterns were also widespread. Although EEG-fMRI does not represent the complete interictal pattern in all patients, the EEG-fMRI correlation pattern included the seizure onset zone in most data sets (83 %). The good overlap between EEG-fMRI and the clinically more relevant seizure onset zone is comparable to the concordance reported by other studies (Grouiller et al. 2011; Thornton et al. 2011; Pittau et al. 2012). Together, these findings indicate that the sensitivity of EEG-fMRI is high. Therefore, we expect an important role for EEG-fMRI regarding decision-making of implantation strategies (Zijlmans et al. 2007).

The specificity of EEG-fMRI appears to be relatively low, since EEG-fMRI yields more areas than detected with interictal ECoG data. The function of these additional regions cannot be validated, because most of them are not covered by subdural grids, particularly in those patients that received acute ECoG. This is a limitation of our comparison, because with subdural grids only neocortical and interhemispheric regions can be targeted and not the more deeply lying structures. Nevertheless, these ECoG data are the best gold standard available for our patient population. Prospective studies, in which the EEG-fMRI results are actually used during the implantation of invasive electrodes, are necessary to determine sensitivity and specificity quantitatively.

One could argue that the high sensitivity is related to the threshold used to

determine statistical significance of detected areas. Applying a more stringent threshold would result in a lower sensitivity and higher specificity. However, we emphasize that the applied FDR threshold of 1 % is already quite stringent. Moreover, from a practical point of view, it is important to keep the purpose of EEG-fMRI in mind. When the goal of EEG-fMRI is to determine the location of the subdural electrode grids, a high sensitivity is more important than a high specificity.

In some patients the presence of an epileptic network could be verified, which is nicely illustrated by the results of patient 1 for whom we could establish that all cortical EEG-fMRI clusters are related to the epileptiform activity as measured by ECoG (see Figure 6.3). Results of this patient further show that one area is related to the early onset of the IEDs, which might indicate that the other concordant areas are related to propagation of these IEDs (Vulliemoz et al. 2009). Similar epileptic network characteristics can also be inferred from the EEG-fMRI results obtained for patients 6, 7, and 10. However, due to the limited spatial ECoG sampling, for most patients it is difficult to assess whether all EEG-fMRI clusters are part of an interictal network. For example, for patient 8 bilateral EEG-fMRI clusters were obtained. The ECoG data show a left temporal onset, but we could not investigate whether the right temporal activations as seen in EEG-fMRI might be related to propagation of the activity.

Our study shows, furthermore, that the shape of the HRF of concordant clusters is variable among patients, therefore suggesting that the use of a standard HRF model may lead to false negative fMRI results (e.g. Josephs et al. 1997; Lu et al. 2007; van Houdt et al. 2010a). Previous studies focused on those areas with the maximal t- or F-statistic (e.g. Kobayashi et al. 2006a; Salek-Haddadi et al. 2006). Our results show that in 7 of the 17 datasets the maximal F-statistic (indicated with the white asterisk in Figure 6.4) was concordant with the ECoG results, confirming the suggestion of the study of Vulliemoz et al. (2009) that the maximal positive t-statistic is not always the area that is most closely related to the presumed epileptiform focus.

It appears to be difficult to decide without a priori information which HRF cluster is clinically important. For instance, we investigated whether the shape of the HRF is predictive for the role within the network, but we did not obtain consistent results. Even the sign of the HRF does not seem to correlate with the level of concordance: both positive and negative HRFs correspond to the early onset areas of IEDs in ECoG. This has also been observed by previous studies and is still a topic of debate (Kobayashi et al. 2006a; Salek-Haddadi et al. 2006; Jacobs et al. 2007; Vulliemoz et al. 2009; Rathakrishnan et al. 2010). One hypothesis explaining negative BOLD responses is the vascular steal phenomenon (Schridde et al. 2008) for BOLD areas with a close spatial relation between positive and negative clusters. Similar to the study of Kobayashi et al. (2006a), we could not confirm that hypothesis, because in only two patients (9 and 10) a positive and a negative HRF cluster were neighboring clusters, and, therefore, other explanations are required (e.g. Schridde et al. 2008). Other characteristics of the HRF shape were also not predictive for concordance. For

instance, both canonical and noncanonical HRF clusters were concordant with the ECoG data and the seizure onset zone, which deviates from the results of the study by Lemieux et al. (2008), who suggested that noncanonical HRFs were most likely not related to the focus of activity. Therefore, it seems that the shape of the HRF is not directly dependent on the underlying electrical epileptiform activity, suggesting a much more complex relation. This relation is an important topic of research also outside the epilepsy research field (e.g. Rosa et al. 2010). For example, some studies suggest that the shape of the HRF is determined by the brain region (Conner et al. 2011) or by the cortical depth (Siero et al. 2011).

For the analysis of the IEDs in the ECoG data we applied an automatic analysis that yields a spatial and temporal pattern for each IED-type. This method was developed for the purpose of EEG-fMRI validation (van Houdt et al. 2012), but might also be useful as a quantitative assessment of clinical invasive EEG data. However, significant patterns were only obtained for the most dominant and frequent spikes (see Table A.1), and not for IEDs that were low in amplitude with respect to the other IEDs or that involved only one or two electrodes. For the purpose of EEG-fMRI validation this is sufficient, because low amplitude and infrequent IEDs are not expected to be visible in the scalp EEG during fMRI scanning. But as a practical clinical tool fine-tuning of the method is still required.

6.4.1 Conclusions

The results of EEG-fMRI are clinically relevant in most patients: EEG-fMRI is usually concordant with one IED-type in the ECoG data and includes the seizure onset zone and resection area. In our opinion, the added value of EEG-fMRI in the presurgical evaluation with respect to other noninvasive techniques is that EEG-fMRI is able to show an interictal network of onset and propagation areas. Furthermore, compared to, for example, high resolution EEG and MEG source localization, EEG-fMRI is able to reveal activations from more deeply lying structures in the brain. For these reasons, there is an important role for EEG-fMRI during surgical planning, especially with regard to the determination of the implantation strategy.

Acknowledgments

This project was supported by the Dutch Epilepsy Foundation (grant 07-16) and the Central Nervous System and Imaging (CSI) project that has received funding from the ENIAC Joint Undertaking (grant no. 120209). The ECoG recordings were performed at University Medical Center Utrecht. We especially acknowledge Cyrille Ferrier and Peter van Rijen for their contribution to the recordings used in this study. Furthermore, we would like to thank Jan Verwoerd from Philips Medical Systems (Best, the Netherlands) for his assistance regarding the MR imaging sequences, Mike

van der Mierden, Marlies Dolmans, and Ine Keulen for the review of the EEG data, Remco Berting and Esther Peeters for their assistance during the EEG-fMRI recordings, and Roy Krijn for technical support.

Appendix: ECoG analysis

The analysis of the ECoG data consists of two parts: the estimation of a spatial and an onset pattern. The analysis is implemented in Matlab (R2009a, The Mathworks, Inc.) and uses several functions of the Fieldtrip toolbox (Oostenveld et al. 2011). For both parts of the analysis, the data was first transformed in a Hjorth derivation to reduce the influence of common sources (Hjorth 1975).

The spatial pattern was determined with the procedure as described in van Houdt et al. (2012), that was developed for the purpose of validation of EEG-fMRI results. The goal of the spatial pattern was to indicate which electrode contacts reflect increased activity during the occurrence of IEDs. The approach is based on the assumption that the mutual correlations between electrodes are increased during epileptiform activity (Bettus et al. 2008). Therefore, a nonlinear association analysis was applied for each ECoG window yielding the maximal association $h^2_{ij}(k)$ and a corresponding time delay $\tau_{ij}(k)$ between electrodes i and j for each 2.5 s window k using equation (A.1) (Lopes da Silva et al. 1989; Pijn et al. 1990; Bartolomei et al. 2001; Wendling et al. 2001; Meeren et al. 2002; Westmijse et al. 2009).

$$h^2_{ij}(k) = \max_{\tau}\left[h^2_{ij}(k \cdot \mathrm{TR}, k \cdot \mathrm{TR} + \tau)\right] \quad -\tau_{\max} \leq \tau \leq \tau_{\max} \quad 0 \leq k \leq K-1 \tag{A.1}$$

$\tau_{\max}$ = 150 ms and K is equal to the number of windows depending on the length of the selected data. Averaging of the $h^2_{ij}(k)$ values for electrode i with all other electrodes reveals an association strength function as shown in equation (A.2).

$$\mathrm{Strength}_i(k) = \frac{1}{N-1}\sum_{j=1, j\neq i}^{N} h^2_{ij}(k) \quad 0 \leq k \leq K-1 \tag{A.2}$$

Next, a GLM framework was applied to reveal which changes in association strength can be explained by the occurrence of IEDs (equation (A.3)).

$$\mathbf{d} = X\mathbf{h} + S\boldsymbol{\phi} + \boldsymbol{\varepsilon} \tag{A.3}$$

In this model, $\mathbf{d}$ represents the association strength function for electrode i. X is the design matrix consisting of the regressors of interest, which are in this formulation the IEDs present in the ECoG data. The required input from the clinician is the timing of IEDs in the ECoG data, which were marked visually and different markers were used for IED-types with different topologies. From these events, an IED density

function was created that was applied as a predictor in the GLM. Different IED density functions were created for different types of IEDs. If multiple IED-types were present, regression analysis was performed for each type separately, while the other IEDs were used as confounders indicated by S. Furthermore, a constant, a linear and quadratic trend were included as confounders. $\mathbf{h}$ and $\boldsymbol{\phi}$ are the corresponding coefficients of interest and non-interest, while $\boldsymbol{\varepsilon}$ is the vector of assumed uncorrelated noise. The regression analysis yielded (1) a correlation value for each electrode, indicating the involvement of each electrode during IEDs relative to the other electrodes; (2) a p-value, indicating whether the correlation is significant. The p-values were transformed into FDR to correct for the number of electrodes. These results were visualized on the anatomical MRI with color-coded dots (see step 6 in Figure 6.1) scaled by the correlation value; nonsignificant correlations were indicated in black (FDR > 5 %).

The second part of the analysis consists of the estimation of an onset pattern (Figure 6.1, step 7-9) based on the delays $\tau_{ij}(m)$ calculated between electrodes i and j from the association analysis for windows m of 1 seconds centered around individual IEDs. These values can be interpreted as the direction of information flow between two signals (Wendling et al. 2001) and were, therefore, used to estimate the moment in time at which an IED was present at electrode i using equation (A.4).

$$t_i(m) = \frac{1}{2N}\left(\sum_j \tau_{ij}(m) - \sum_j \tau_{ji}(m)\right), \quad m = 1 \cdots M \tag{A.4}$$

in which M is equal to the number of IEDs marked in the ECoG data. Thus, for each event an onset pattern was estimated. The estimated time points are not absolute values, but are relative with respect to the other electrodes due to the assumption that $\sum_i t_i = 0$. To exclude nonsignificant correlations (i.e. time delays that are not related to IEDs), time delays were only included in the model if $h^2_{ij}(m)$ was larger than the mean and three times the standard deviation of the association values for all time shifts (i.e. the association curve as function of time shifts τ, defined as $h^2_{ij}(k \cdot \mathrm{TR}, k \cdot \mathrm{TR} + \tau)$). The color of the dots is scaled to estimated time points: more white means that the activity was earlier present at that electrode than red/black colored electrodes. Note that, in theory the delays of the spatial pattern (see step 2 in Figure 6.1) could have been used for the estimation of the onset pattern. However, in practice it appeared that the onset patterns may vary slightly between IEDs, even if the same electrodes are involved with the spatial pattern. If multiple IEDs are present within a window, which is often the case for 2.5 s windows, the delays may reflect mixed results. Therefore, we decided to repeat the analysis for shorter windows that are centered around IEDs. Only windows where one IED was present were taken into account.

Appendix: Supplementary Table 1

Table A.1: Summary of EEG-fMRI and interictal ECoG Results. For all IED-types that were present in the ECoG data (column 2), the spatial correlation pattern (column 3) and onset pattern (column 4) are summarized. Furthermore, for each IED-type present during the EEG-fMRI recording (column 5) and for each HRF cluster (column 6) the brain regions involved are indicated (column 7). The last columns indicate the concordance of each HRF cluster with the ECoG spatial and onset patterns and with the resection area.

Patient	Interictal ECoG			EEG-fMRI			Concordance of EEG-fMRI		
	IEDs max (No.)	Spatial Pattern	Early Onset	IEDs max (No.)	fMRI Cluster No. (No. voxels)	Brain Regions[3]	Spatial	Onset	Resection
1	1 (390)	TL-l; P-l; TM-l	TL-l	1 (87)	1 (64)	TM-l; B-l	C+	D	No
	2 (681)	∅	∅		2 (111)	Ins-l; FL-l; FO-l	U	-	No
					3 (79)	Ins-l; TL-l; TM-l	C+	C+	No
					4 (16)	∅	-	-	No
					5 (41)	TL-l	C	D	Yes
					6 (86)	TL-l	C	D	No
2	1 (52)	TL-l	TL-l	1 (71)	1 (128)	TL-l	C	C	Yes
	2 (119)	∅	∅		2 (42)	∅	-	-	No
					3 (79)	C-r; FO-r	U	-	No
3	1 (200)	FL-l; IH-l	variable	1 (49)	1 (30)	FO-l	C	C	Yes
	2 (258)	C-l			2 (19)	∅	-	-	No
	3 (146)	∅	∅						
4	1 (115)	IH-r	IH-r	1 (122)	1 (410)	IH-r; FO-r; FL-r	$C_{1,2}$+	$C_{1,2}$+	Yes
	2 (73)	IH-r	IH-r		2 (3355)	O-b; C-b; IH-b; Ins-r; FL-b; +W	U	-	No
					3 (2186)	Ins-r; TL-l; TM-b; IH-b; O-l; +W	U	-	No
					4 (2385)	Ins-b; C-b; TL-b; IH-b; P-b; +W	U	-	No
					5 (1670)	B-r; TM-b; IH-b; Ins-r; P-l; +W	U	-	No
5	1 (46)	TM-l; TL-l; IH-l	TM-l	1 (28)	1 (183)	FO-l; IH-r; TL-r; FL-b; C-r	U	-	-
	2 (48)	O-l	O-l		2 (604)	B-r; TL-r; C-b; FL-b; P-b; +W	D	-	-
	3 (76)	TL-l			3 (2647)	TM-l; TL-l; Ins-l; IH-l; C-l; +W	C_1+, C_3+	C_1+, C_3+	-
6	1 (44)	TL-r; P-r; FL-r; FO-r	TL-r / P-r / FL-r	1 (155)	1 (646)	FO-r; FO-l; IH-b; Ins-b; FL-b; +W	C+	D	No
					2 (685)	Ins-b; B-b; IH-b; FO-b; FL-b; +W	C+	C+	Yes
					3 (70)	O-l; TL-l; TL-r	U	-	No
7	1 (107)	FO-r; FL-r; IH-r	IH-r	1 (92)	1 (58)	IH-r; B-r	C+	C+	Yes
					2 (69)	O-b; Ins-l	U	-	No
					3 (563)	FL-r; IH-r; P-r; FL-l; C-r; +W	C+	D	No

[3]the activated voxels are ordered based on the percentage activation per brain region (i.e. number of activated voxels in a brain region divided by the total number of voxels in a brain region). If more than 5 brain regions were involved, this is indicated with "+W" (if these activations consists of more than 0.5 % of the total brain region).

Table A.1: continued

Patient	Interictal ECoG			EEG-fMRI			Concordance of EEG-fMRI		
	IEDs max (No.)	Spatial Pattern	Early Onset	IEDs max (No.)	fMRI Cluster No. (No. voxels)	Brain Regions	Spatial	Onset	Resection
					4 (1267)	O-r; P-b; IH-b; FL-r; FO-r; +W	U	-	No
					5 (125)	P-b; O-r	U	-	No
8	1 (253)	TL-l	TL-l	1 (9)	1 (753)	TL-r; TL-l; P-r; IH-b	C_1+, C_2+	C_1+, C_2+	Yes
	2 (222)	TL-l; FO-l; TM-l	TM-l		2 (158)	Ins-l; FO-l; TL-l	C_2	C_2	No
	3 (92)	∅	∅		3 (318)	TL-r; TM-r; Ins-l; C-l	U	-	No
	4 (14)	∅	∅						
	5 (14)	∅	∅						
	6 (39)	∅	∅						
	7 (38)	∅	∅						
9	1 (300)	P-l; C-l; TL-l	P-l	1 (34)	1 (195)	C-b; TL-l	$C_{1,2}$+	$C_{1,2}$+	Yes
	2 (49)	TL-l; P-l, FL-l	∅		2 (181)	Ins-r; TM-r	U	-	No
					3 (62)	C-l; P-l	$C_{1,2}$+	$C_{1,2}$+	Yes
10	1 (229)	P-l; TL-l; FL-l	P-l	1 (10)	1 (110)	∅	-	-	-
	2 (80)	∅	∅		2 (1155)	Ins-b; FL-l; IH-l; B-b; TL-l; +W	C_1+	D	-
	3 (142)	∅	∅		3 (764)	TL-l; FO-b; B-r; IH-l; FL-r; +W	U	-	-
					4 (1126)	FO-b; TL-b; Ins-b; FL-l; B-b; +W	C_1+	D	-
11	1 (39)	P-r; TL-r	TL-r	1 (10)	1 (250)	B-b; FL-l; TL-l; FO-b; IH-l	U	-	No
	2 (51)	TM-r; FO-r; IH-r	TM-r		2 (69)	TL-r; IH-b; B-r	C_1+, C_3+	C_1+	Yes
	3 (230)	C-r; P-r; TL-r; TM-r	P-r		3 (1140)	TM-r; FO-r; Ins-r; FO-l; C-l; +W	C_2+, C_3+	C_2+	Yes
	4 (290)	∅	∅						
	5 (20)	∅	∅						
	6 (51)	∅	∅						
12	1 (31)	FL-l; FO-l; IH-l	FL-l / IH-l	1 (10)	1 (139)	FO-r; FO-l; FL-l	C+	D	Yes
	2 (47)	∅	∅		2 (23)	∅	-	-	No
					3 (342)	FO-l; IH-l; FO-r; FM-l; TL-l; +W	C+	C+	Yes
13	1 (12)	IH-r; FL-r; TL-r	IH-r / FL-r	1 (12)	1 (742)	Ins- b; FL-b; C-b; TL-r; FM-b; +W	C+	C+	Yes
					2 (457)	Ins-b; FL-b; C-b; IH-b; B-r; +W	C+	C+	Yes
					3 (189)	IH-b; FL-r; C-b	C+	C+	Yes
					4 (33)	∅	-	-	No
					5 (8)	∅	-	-	No
14	1 (18)	TL-l; TM-l	TM-l	1 (18)	1 (836)	FL-b; TL-r; O-l; Ins-l; B-b	U	-	No
	2 (8)	TM-l	TM-l		2 (731)	FO-b; B-b; TM-b; TL-b; IH-r	U	-	No
					3 (816)	TM-r; FO-b; TL-b; P-r; Ins-r; +W	C+	C+	Yes
					4 (969)	FO-b; TM-r; Ins-r; TL-r; IH-b; +W	U	-	No
					5 (1535)	FO-b; B-r; Ins-r; TM-l; TL-l; +W	C+	D	No

Table A.1: continued

Patient	Interictal ECoG			EEG-fMRI			Concordance of EEG-fMRI		
	IEDs max (No.)	Spatial Pattern	Early Onset	IEDs max (No.)	fMRI Cluster No. (No. voxels)	Brain Regions	Spatial	Onset	Resection
				2 (12)	1 (250)	FO-r; FL-r; FO-l	U	-	No
					2 (101)	FL-l; FL-r	U	-	No
					3 (382)	FO-l; FO-r; FL-l; TL-r	U	-	No
					4 (325)	FO-l; TL-l	C+	D	No
15	1 (6)	TM-r	TM-r	1 (9)	1 (406)	B-b; TM-r; O-r; IH-l; TL-l; +W	$C_{1,2}$+	C_1+	Yes
	2 (57)	TL-r; TM-r; P-r; C-r	P-r; TL-r		2 (874)	B-l; P-b; FL-b; IH-b; C-b; +W	$C_{2,4}$+	$C_{2,4}$+	No
	3 (27)	TL-r	TL-r		3 (510)	IH-b; P-l; C-b; Ins-r; FL-l; +W	$C_{2,4}$+	D	No
	4 (9)	TL-r; IH-r; O-r, P-r	P-r; TL-r		4 (661)	TM-r; Ins-b; FO-r; TL-r; IH-r; +W	$C_{1,2,3,4,5}$+	$C_{1,2,3,4,5}$+	Yes
	5 (46)	TL-r, P-r	TL-r		5 (1435)	Ins-r; C-b; TM-r; B-r; TL-b; +W	$C_{1,2,3,4,5}$+	$C_{1,2,3,4,5}$+	Yes
	6 (13)	∅							
	7 (25)	∅							
16	1 (21)	∅	∅	1 (55)	1 (344)	TL-l; FO-b; Ins-l; O-l; FL-b; +W	∅	∅	Yes
	2 (55)	∅	∅		2 (3184)	FL-b; IH-b; FM-r; TL-r; P-r; +W	∅	∅	No
					3 (2953)	IH-b; TL-b; FL-l; B-b; FO-l; +W	∅	∅	No

Abbreviations: l = left; r = right; b= bilateral (if symmetric); TL = lateral temporal regions; TM = mesial temporal region; FL = inferior, medial, and superior frontal gyri; FO = orbitofrontal region; IH = interhemispheric region; C = central region; P = parietal region; O = occipital region; B = basal ganglia and thalamus; Ins = insular region; ∅ (ECoG) = no significant results; ∅ (EEG-fMRI) = activated voxels were located outside the above specified brain regions (e.g. white matter, ventricles, cerebellum).